

# Cellulose nanocrystals reinforced environmentally-friendly waterborne polyurethane nanocomposites

(<http://dx.doi.org/10.1016/j.carbpol.2016.06.069>)

Arantzazu Santamaria-Echart, Lorena Ugarte, Clara García-Astrain, Aitor Arbelaitz,  
Maria Angeles Corcuera\*, Arantxa Eceiza\*

Group 'Materials+Technologies', Department of Chemical and Environmental Engineering, Polytechnic School,  
University of the Basque Country, Pza Europa 1, Donostia-San Sebastian 20018, Spain

## ABSTRACT

Focusing on eco-friendly materials, cellulose nanocrystals (CNC) have gained attention as nanoreinforcement due to their exceptional properties conferred by the elevated length/diameter aspect ratio and high specific mechanical properties. Furthermore, their water dispersibility makes them suitable nanoreinforcements for their incorporation in waterborne polyurethanes (WBU). The possibility of tailoring the properties by varying the composition and nature of the reagents, opens the opportunity for a wide range of applications. Therefore, in this work a WBU was synthesized for the preparation of nanocomposite films with different CNC content and the properties of the films were analyzed. The effective incorporation of CNC resulted in an increase in moduli and stress at yield besides in an increased thermomechanical stability, reaching the percolation threshold at a 3 wt% CNC as determined theoretically. Nevertheless, above the percolation threshold, the presence of agglomerates reduced slightly these values. The prepared nanocomposites showed increased hydrophilicity after CNC addition.

## 1. Introduction

Polyurethanes are a wide family of block copolymers composed by a macrodioil as soft segment (SS) and an isocyanate and low molecular weight chain extender diol as hard segment (HS). The incompatibility between both segments leads to their separation in microphases (Rueda, Fernandez d'Arlas, Corcuera, & Eceiza, 2014). Furthermore, varying segment content as well as the composition and nature of the reagents, different polyurethanes can be tailored (Tharcis, Badel, Jéol, Fleury, & Méchin, 2016). In this way, different soft and hard segments molecular architectures, both crystalline and amorphous, can be obtained, leading to polyurethanes with diverse properties, opening the way for a wide range of applications such as coatings, adhesives, or in printing or medicine (Leitsch, Heath, & Torkelson, 2016; Mao et al., 2015; Mo et al., 2015; Si, 2016). Recently, the increase of global environmental awareness, the aim of reducing organic volatile compounds and the guidelines to tackle climate change, have promoted the research focused on waterborne systems (Framework convention on climate change, 2015). Thereby, waterborne polyurethanes (WBU) have gained attention due to their ability to assemble in stable particles in water dispersions by the addition of a covalently bonded internal emulsifier (Chattopadhyay & Raju, 2007; Nelson & Long, 2014). In this way, besides obtaining environmentally-friendly polyurethanes, water dispersible reinforcement incorporation such as cellulose nanocrystals (CNC) is facilitated (Gopiraman et al., 2016; Kushwaha, Avadhani, & Singh, 2015; Mariano, El Kissi, & Dufresne, 2014; Zhang et al., 2014; Zhou et al., 2016).

Cellulose is one of the most abundant polymers in nature, which can be obtained from different sources like plants, bacteria or tunicates that, attending to the applied treatments lead to diverse forms like fibers or crystals, from the macro to the nanoscale (Eichhorn et al., 2010; Hribernik et al., 2016; Kunaver, Anzlovar, & Zagar, 2016; Tuzzin, Godinho, Dettmer, & Zattera, 2016; Xiang, Mohammed, & Baharuddin, 2016). Focusing on cellulose nanocrystals, the isolation of CNC commonly proceeds by acid hydrolysis with sulfuric or hydrochloric acid ( $H_2SO_4$  or  $HCl$ ) (Dong, Revol, & Gray, 1998), leading to rod-like shape crystalline nanoentities which exhibit unique advantages in terms of biodegradability, recyclability, renewability, biocompatibility and low cost (Mondragon et al., 2014). Furthermore, the elevated length/diameter (L/D) aspect ratio and the high specific mechanical properties, favor their use as effective reinforcements in nanocomposites (Azizi Samir, Alloin, & Dufresne, 2005). Moreover, the negatively charged sulfate groups anchored to CNC during the  $H_2SO_4$  hydrolysis favor the formation of stable dispersions of CNC in water (Beck, Bouchard & Berry, 2012), without requiring additional drying steps which difficult their redispersion, even in water (Beck et al., 2012). Therefore, environmentally sustainable nanocomposites can be pursued based on non-dried CNC aqueous dispersions and water dispersible polymers. In this way, the compatibility between both components is ensured, without requiring chemical modifications or the addition of surfactants (Mariano et al., 2014). Thereby, the opportunity of dispersing CNC in WBPU dispersion is presented as a sustainable attractive via for obtaining nanocomposites. In this work a stable WBPU dispersion with high hard segment content was synthesized. Furthermore, water dispersed CNC with an elevated L/D aspect ratio were isolated and employed for the preparation of WBPU-CNC nanocomposite films. The effect of different CNC contents over the final properties of the obtained films was analyzed in terms of physicochemical, thermal, mechanical and thermomechanical properties as well as in terms of hydrophilicity and morphology.

## 2. Experimental

### 2.1. Materials

For waterborne polyurethane matrix synthesis, difunctional poly ( $\epsilon$ -caprolactone) diol (PCL) ( $M_w = 2000 \text{ g mol}^{-1}$ ), purchased from BASF was employed as soft segment. 1,4-Butanediol (BD), used as chain extender, and 2,2-bis(hydroxymethyl)propionic acid (DMPA), used as internal emulsifier, were provided from Aldrich. PCL, BD and DMPA were dried under vacuum at 50 °C for 4 h prior to their use. Isophorone diisocyanate (IPDI), supplied from Bayer, and dibutyltin dilaurate (DBTDL), provided from Aldrich, were used as received. Tetrahydrofuran (THF) was employed to adjust viscosity and triethylamine (TEA) as neutralizer, both purchased from Aldrich. THF and TEA were dehydrated with hydralan-molecular Sieve 0.3 nm (water adsorption capacity of 15%), supplied by Fluka, and previously dried at 55 °C under vacuum for 1 day. Microcrystalline cellulose (MCC) powder was supplied from Aldrich and concentrated sulfuric acid (96%) was provided from Panreac.

### 2.2. Preparation of waterborne polyurethanes

Considering PCL as SS and IPDI, DMPA and BD as HS, WBPU containing 48 wt% of HS was synthesized by two step polymerization with a PCL/DMPA/IPDI/BD molar ratio of 0.5/0.5/3.15/2 following a previously reported protocol (Santamaría-Echart et al., 2015). The reaction was carried out in a 250 mL four-necked flask equipped with a mechanical stirrer, thermometer, condenser and nitrogen inlet within a thermostatized bath. The reaction progress was determined by dibutylamine back titration method according to ASTM D 2572-97. In the first step, PCL, IPDI and 0.1 wt% of DBTDL were reacted at 90 °C for 5 h and then DMPA was incorporated. Afterwards, BD was added for the chain extension step. The system was cooled until room temperature while viscosity was controlled by adding low amounts of THF and TEA was added in order to neutralize all carboxylic groups of DMPA. Thereafter, the dispersion step was carried out by adding deionized water (DI) dropwise, under vigorous stirring and THF was removed in a rotary evaporator obtaining a dispersion with about 25 wt% solid content. A scheme of the synthesis reaction process is shown in supplementary material.

### *2.3. Isolation of cellulose nanocrystals*

The isolation of CNC was carried out by H<sub>2</sub>SO<sub>4</sub> hydrolysis of the amorphous regions of MCC, following a previously reported method (Santamaría-Echart et al., 2016). Briefly, the hydrolysis was carried out by mixing MCC with H<sub>2</sub>SO<sub>4</sub>(64 wt%) at 45 °C for 30 min. Then, the suspension was diluted with DI and washed by successive centrifugation cycles. The resulting suspension was dialyzed against DI water until pH 5–6 was reached and a CNC suspension with about 0.5 wt% was obtained. During the hydrolysis some sulfate groups are anchored in the CNC surface leading to electrostatic repulsion between CNC, which improves their dispersibility in polar solvents.

### *2.4. WBPU-CNC nanocomposites preparation*

WBPU-CNC nanocomposites were prepared by casting. CNC suspension was sonicated for 1 h, and after the addition to WBPU, the mixture was sonicated for another 1 h. The resulting mixture was poured in Teflon mould and dried in a climatic chamber at 25 °C and 50% of relative humidity for one week and in a vacuum oven at 25 °C for 3 days. Varying the total weight content of CNC, films with a thickness of about 0.4 mm were prepared by adding 0.5, 1,3 and 5 wt% of CNC to WBPU. The matrix and the nanocomposites were denoted as WBPU, WBPU-0.5, WBPU-1, WBPU-3 and WBPU-5 respectively.

### *2.5. Characterization*

Particle size and distribution of WBPU dispersion was determined by dynamic light scattering (DLS) in a BI-200SM goniometer from Brookhaven. A luminous source of He-Ne laser (Mini L-30, wavelength  $\lambda$ = 637 nm, 400 mW) and a rotary arm equipped with a detector (BI-APD) were used for the measurement of the intensity of the dispersed light at 90° at 25 °C. The sample, analyzed in triplicate, was prepared by diluting WBPU dispersion in ultrapure water. The concentration of sulfate groups

anchored to the CNC surface was determined by conductometric titration, using a Crison EC-Meter GLP 31 conductometer calibrated with 147  $\mu\text{S cm}^{-1}$ , 1413  $\mu\text{S cm}^{-1}$  and 12.88 mS  $\text{cm}^{-1}$  standards. Samples were measured in triplicate at 25 °C using NaOH and HCl 10 mM for the titration. The concentration of sulphate groups was also determined by elemental analysis in a Euro EA3000 Elemental Analyzer of Eurovector. Samples were measured by SCAB.PE.29.PR.10.02 method in solid state.

The characteristic functional groups of CNC, WPU and the were analyzed by Fourier transform infrared (FTIR) spectroscopy using Nicolet Nexus spectrometer provided with a MKII Golden Gate accessory (Specac) with a diamond crystal at a nominal incidence angle of 45° and ZnSe lens. Spectra were recorder in attenuated reflection (ATR) mode between 4000 and 650  $\text{cm}^{-1}$  averaging 64 scans with a resolution of 8  $\text{cm}^{-1}$ . Thermal properties of films were studied by differential scanning calorimetry (DSC) using a Mettler Toledo 822eequipment, provided with a robotic arm and an electric intracooler as the refrigerator unit. Aluminum pans containing samples (5-10 mg) were heated from - 80 to 180°C at a scanning rate of 20°C  $\text{min}^{-1}$  in nitrogen atmosphere. Glass transition temperature was determined as the inflection point of the heat capacity change, whereas melting temperature and enthalpy were established as the maximum and the area under the endotherm peak, respectively.

Mechanical properties were determined in a MTS insight 10testing machine provided with a 250 N load cell and pneumatic grips to hold the samples. Samples were cut (8 mm in length, 2.5 mm in width and 0.4 mm in thickness) and tested at a crosshead speed of 50  $\text{mm min}^{-1}$  at room temperature. Thermomechanical behavior was analyzed by dynamic mechanical analysis (DMA) using an Eplexor 100 N analyser, Gabo equipment. Samples were performed in tapping mode from - 100 to 120 °C at a scanning rate of 2 °C  $\text{min}^{-1}$  with an static strain of 0.05% and operating frequency of 1 Hz. Water contact angle (WCA) values were measured in a Data-physics OCA20 equipment at room temperature. For each sample six measurements were averaged by dropping 2  $\mu\text{L}$  of deionized water droplets over the nanocomposites surface. Water absorption (WA) measurements were carried out by weighing 15–20 mg of nanocomposite films immersed in deionized water at 25 °C. Water absorption percentage was determined by means of the following equation:

$$W (\%) = \frac{W_t - W_0}{W_0} \times 100$$

where  $W_t$  and  $W_0$  are referred to the weight at time t and the initial weight respectively. Morphology of the nanocomposites was analyzed by atomic force microscopy (AFM) in tapping mode using a Nanoscope IIIa scanning probe microscope (MultimodeTMDigital instruments) with an integrated force generated by cantilever/silicon probes, applying a resonance frequency of about 180 kHz. Cantilevers had a tip radius of 5–10 nm and were 125  $\mu\text{m}$  long. Samples were prepared by spin-coating (Spincoater P6700) at 2000 rpm for 130 s by casting a droplet of nanocomposites dispersion on glass supports.

### **3. Results and discussion**

The particle size and distribution were determined by DLS. The particle size resulted to be  $52.3 \pm 0.5$  nm with a narrow polydispersity of  $0.08 \pm 0.05$  contributing to the stability of the WBPU. It is worth noting that small particle sizes favor the storage stability of the dispersions. During water addition process, WBPU chains adopt a core-shell particle conformation, where the segment containing the ionic group is fixed in the shell, and the hydrophobic segment forms the core. In this way, the ionic groups form an electrochemical double layer with TEA counter ion conferring stability to the dispersion (Bullermann, Friebel, Salthammer, & Spohnholz, 2013). In general, small particles favor the formation of thicker double layers, attributable to the effectiveness of the conformed structures, leading to more stable systems (Gaddam & Palanisamy, 2016). Thereby, considering the small particles obtained, the synthesized WBPU resulted visually stable over six months, presenting no evidences of agglomerations, and showing a pH of 8.6. The characterization of isolated CNC showed a sulfur content around 1.25% and a diameter and length about  $5.4 \pm 1.5$  nm and  $167 \pm 31$  nm, respectively, resulting in L/D aspect ratio of about 31 (Santamaria-Echart et al., 2016).

Polyurethane structure has been determined by  $^1\text{H}$  and  $^{13}\text{C}$  NMR analysis, and the spectra are shown in supplementary material (SI). Nanocomposites characteristic functional groups have been characterized by FTIR and the spectra are shown in Fig. 1. Two typical regions are differentiated related to N-H stretching vibration of urethane and OH groups of CNC and carbonyl (C=O) stretching vibration of urethane linkages. In the stretching region between 3100 and 3600  $\text{cm}^{-1}$ , a band around 3340  $\text{cm}^{-1}$  is observed in WBPU and nanocomposites attributed to hydrogen-bonded N-H groups, whereas CNC shows two peaks at 3332 and 3287  $\text{cm}^{-1}$  referred to OH groups stretching vibration (Santamaria-Echart et al., 2016). In nanocomposites, an increase in the peak intensity can be appreciated as CNC content is increased, related with the overlapping with the OH stretching vibration band observed in the neat CNC spectrum. With the purpose of analyzing WBPU and nanocomposites C=O characteristic bands, an amplification of the spectrum is showed in the inset of Fig. 1. The band about 1720  $\text{cm}^{-1}$  is related with the free urethane C=O groups, whereas the shoulder about 1700  $\text{cm}^{-1}$  is attributable to hydrogen bonded urethane C=O groups. It has been observed that free C=O groups band shifts to higher wavenumbers whereas the shoulder referred to hydrogen bonded C=O groups broadens, suggesting the generation of new WBPU-CNC interactions.

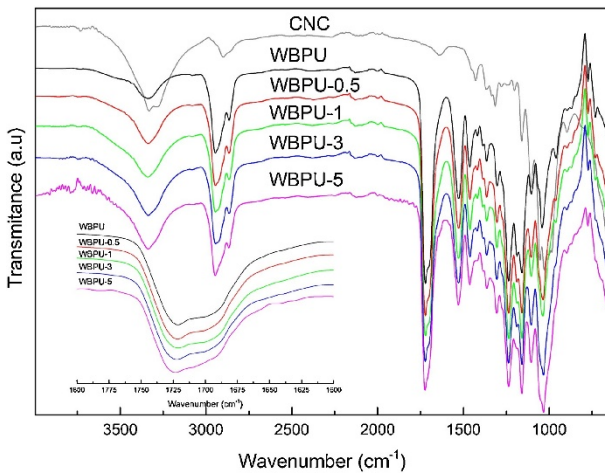


**Fig. 1.** FTIR spectra of CNC, matrix and nanocomposites.

DSC thermograms of the nanocomposites are displayed in Fig. 2 and soft segment glass transition temperature ( $T_{gss}$ ), melting temperature ( $T_{mss}$ ) and enthalpy ( $\Delta H_{mss}$ ) values obtained from the curves are shown in Table 1.

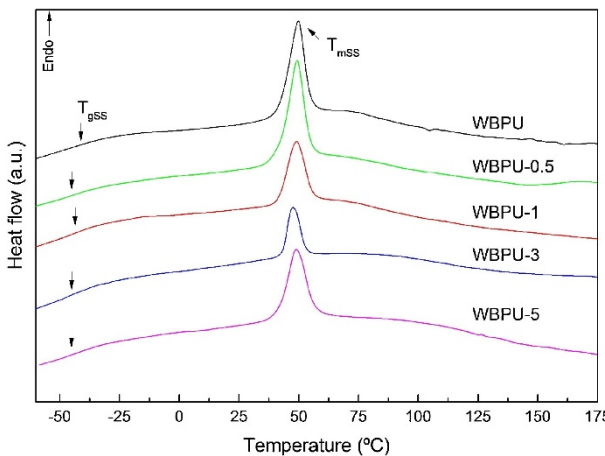


**Fig. 2.** DSC thermograms of matrix and nanocomposites

**Table 1.** Thermal properties of matrix and nanocomposites.

Sample	$T_{gss}$ (°C)	$T_{mss}$ (°C)	$\Delta H_{mss}$ (J g <sup>-1</sup> )	$X_{css}$
WBPU	-43.2	49.8	9.9	1
WBPU-0.5	-47.8	49.1	11.1	1.13
WBPU-1	-45.8	49.1	7.1	0.72
WBPU-3	-47.5	47.5	4.1	0.43
WBPU-5	-47.5	48.8	9.0	0.96

A slight decrease in  $T_{gss}$  of the nanocomposites comparing with the matrix has been observed. The addition of CNC can interfere in the matrix interactions providing greater mobility to chains (Liu, Cui, Shang, Wang, & Song, 2013). Regarding the endothermic peak, it is possible to calculate the relative soft segment crystallinity ( $X_{css}$ ) with respect to the neat WBPU, in order to obtain more accurate information about the crystallinity

of the SS in each composite.  $\chi_{CSS}$  has been determined by means of the following equation (Wunderlich, 2005):

$$\chi_{CSS} = \frac{\Delta H_m}{\omega \cdot \Delta H_{100}}$$

where  $\Delta H_{100}$  is the melting enthalpy of the neat WBPU,  $\omega$  the weight fraction of WBPU in the nanocomposite and  $\Delta H_m$  the melting enthalpy of the corresponding nanocomposite. At low reinforcement content (0.5 wt%), an increase of the  $\chi_{CSS}$  can be observed due to the formation of new interactions between CNC and the matrix, comparing with the neat polyurethane, which promotes the ordering of soft domains (Rueda et al., 2013). Otherwise as CNC content is increased, a decrease in  $\chi_{CSS}$  is observed. The creation of new WBPU-CNC interactions and the greater amount of reinforcement gradually hinder soft domains crystallization (Benhamou, Kaddami, Magnin, Dufresne, & Ahmad, 2015; Saralegi et al., 2013). In the case of 5 wt% of CNC, a raise in  $\chi_{CSS}$  has been observed instead, reaching a value similar to WBPU matrix. The possible formation of agglomerates tends to prevail CNC-CNC interactions over CNC-WBPU interactions, favoring the ordering of soft segment in crystalline domains.

Mechanical behavior of nanocomposites is displayed in Fig. 3 and stress at yield ( $\sigma_y$ ), stress at break ( $\sigma_b$ ), moduli (E) and strain at break ( $\epsilon$ ) values obtained from the curves are summarized in Table 2. It has been observed that, in general, nanocomposites showed higher moduli and low strain at break values comparing with the matrix, due to the reinforcement effect of CNC. The high modulus value observed in the case of 0.5 wt% of CNC could be related to the higher crystallinity observed by DSC.

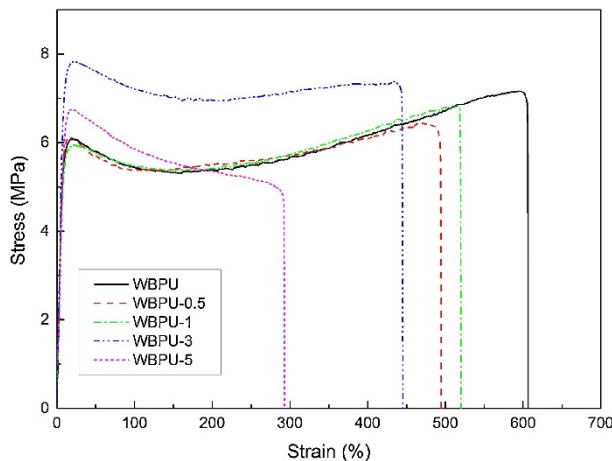


**Fig. 3.** Stress strain curves of matrix and nanocomposites.

**Table 2.** Mechanical properties of matrix and nanocomposites.

Sample	Modulus (MPa)	Stress at yield (MPa)	Stress at break (MPa)	Strain at break (%)
WBPU	76.4±3.5	6.1±0.5	7.3±0.5	612±28
WBPU-0.5	83.6±2.0	5.7±0.4	6.5±0.1	501±38
WBPU-1	79.0±0.9	5.7±0.8	6.4±0.5	472±29
WBPU-3	88.1±2.5	8.3±0.7	7.4±0.6	391±58
WBPU-5	73.9±5.9	6.5±0.1	5.1±0.2	220±74

Taking into account the reinforcement L/D aspect ratio, the theoretical volume fraction of CNC ( $V_{Rc}$ ) needed in order to reach the percolation threshold in the nanocomposite has been estimated by means of the equation (Habibi, Lucia, & Rojas, 2010):

$$V_{Rc} = \frac{0.7}{(L/D)}$$

Considering 1.08 and 1.5 g cm<sup>-1</sup> WBPU and CNC densities respectively (Cao, Dong, & Li, 2007), values of 2.26 vol% and 3.2 wt% were obtained. Regarding the nanocomposites with 3 wt% of CNC, the highest modulus and stress at yield values were observed (showing an improvement of 16 and 36% in E and  $\sigma_y$  respectively, comparing with the matrix). This fact supports the theoretically calculated value. At higher CNC content (5 wt%), though an improvement in stress at yield is observed, the moduli and stress and strain at break values decreased in the nanocomposite. Above the theoretical percolation threshold, the possible presence of some agglomerates could reduce WBPU-CNC interfacial area, hindering stress transfer in the nanocomposite (Gao et al., 2012).

The thermomechanical behavior of the films was studied by analyzing the evolution of storage modulus (E') and Tanδ curves as a function of temperature, which is shown in Fig. 4. At low temperatures, in the glassy state, nanocomposites show similar E' values comparing with the matrix. By increasing temperature, between -50 and -30 °C, a decrease in E' values is observed associated with the  $T_{gss}$  of the matrix, as observed in DSC results. This transition is also reflected as a peak in Tanδ curves which becomes less intense with CNC addition, except for 5 wt%. This fact could be related with the WBPU-CNC interactions, which would reduce the amount of mobile chains in the matrix (Ly, Thielemans, Dufresne, Chaussy, & Belgacem, 2008; Rueda et al., 2011). In the case of WBPU-5, the possible formation of some aggregates, as suggested by mechanical properties results, promotes CNC-CNC interactions, providing again greater mobility to WBPU chains. In the rubbery plateau, higher E' values are observed in the nanocomposites comparing with the matrix, attributable to the effective reinforcement of CNC (Pei, Malho, Ruokolainen, Zhou, & Berglund, 2011). In this region, as temperature increases, a progressive drop in E' values is observed and, as it approaches to the soft segments melting region, the WBPU-CNC network collapses and the film

flows (Auad, Mosiewicki, Richardson, Aranguren, & Marcovich, 2010). Nevertheless, CNC addition retards even up to 10 °C the thermomechanical stability of nanocomposites, except again for 5 wt%.

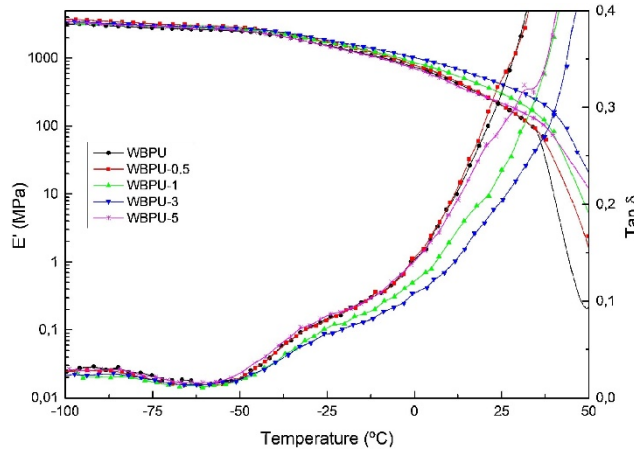


**Fig. 4.** Storage modulus and  $\tan\delta$  curves of matrix and nanocomposites

Hydrophilicity results of nanocomposites analyzed by water contact angle values and water absorption measurements are shown in Fig. 5. Contact angle measurement is a suitable technique in order to comprehend the affinity of the materials surface with liquids (Kushwaha, Avadhani, & Singh, 2014). Regarding the WCA values, it is considered that hydrophobic surfaces present higher values than 90°, while hydrophilic surfaces are characterized by presenting lower WCA values (Yilgör, Yilgör, & Wilkes, 2015). In this case, WBPU matrix presents a considerably hydrophobic character which is reduced as CNC content is increased, even around 15° for WBPU-5. These results are attributable to the greater hydrophilicity of the nanocomposites provided by the hydrophilic character of CNC (Ashori, Babaee, Jonoobi, & Hamzeh, 2014; Hubbe, Gardner, & Shen, 2015; Ly et al., 2008). Similar deviation values of 2–3° can be observed in the nanocomposites, which suggest that the films possess a homogeneous surface. Furthermore, student's t-test was performed comparing each nanocomposite against WBPU matrix in order to assure whether the variation in WA values is significant. Considering a statistical significance ( $\alpha$ ) of 0.05, p-values of  $4.99 \times 10^{-3}$ ,  $3.29 \times 10^{-6}$ ,  $1.37 \times 10^{-3}$  and  $2.80 \times 10^{-5}$  have been obtained for WBPU-0.5, WBPU-1, WBPU-3 and WBPU-5, respectively. The fact that nanocomposites show p-values lower than  $\alpha$ , indicates that they present a significant variation in WA values in comparison with the matrix. This tendency can be also observed in water absorption values where WA values increase with the increase of CNC content. Water molecules diffuse through the material and tend to approach the WBPU-CNC interface where CNC are located, (Benhamou et al., 2015) and which results greater as CNC content increase. In addition, once the percolation threshold is established, the diffusion of water molecules is promoted (Mariano et al., 2014), and that could be the reason of the considerable increase in WA values observed for the sample with 3 wt% of CNC. At higher CNC content, for WBPU-5, the possible aggregates formed in the nanocomposite, would

tend to locate CNC in certain areas, decreasing WA values respect to WBU-3. However, it is worth noting that a decrease in WA values can be observed overtime in some of the samples. It is true that in the nanocomposite of 5 wt% of CNC lower water absorption values are observed comparing with nanocomposite of 3 wt%, but nevertheless, the beginning of the weight loss phenomena is sharper. In the case of 3 wt% of CNC, the formation of the network confers more stability to the film, contributing to a more controlled weight loss of the nanocomposite. However, the agglomerates formed in the case of 5 wt%, result in located weak points where water can access more easily, which could provoke weight loss.

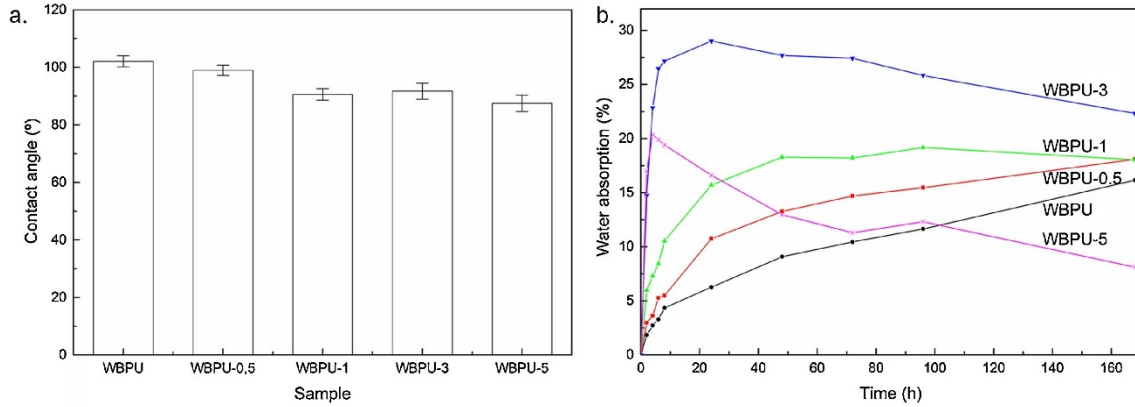


**Fig. 5.** (a) Water contact angle and (b) water absorption measurements of matrix and nanocomposites.

The morphology of the matrix and CNC dispersion in the nanocomposites have been analyzed by AFM, and the height and phase images are shown in Fig. 6.

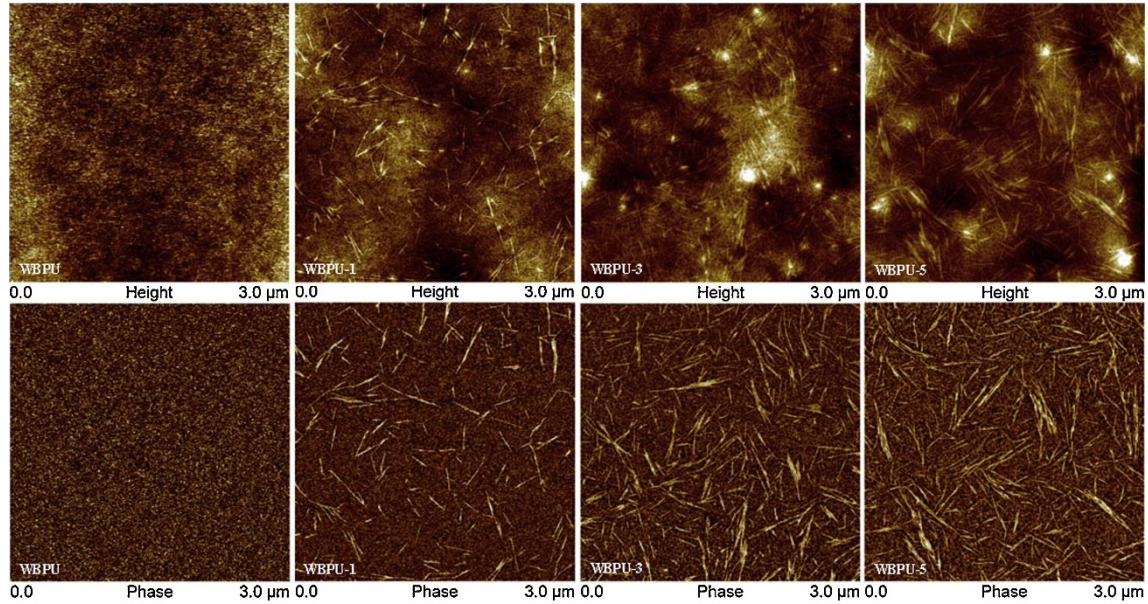


**Fig. 6.** AFM height and phase images of matrix and nanocomposites.

In the matrix, dark and bright regions can be appreciated, attributed to the amorphous and crystalline domains, respectively (Schön et al., 2011). Regarding the

nanocomposites, similar morphological structure has been observed comparing with the matrix, suggesting that CNC barely alter WPU morphology. Furthermore, greater quantity of CNC can be observed as CNC content is increased, showing an effective homogeneous dispersion of CNC in the matrix. (Liu, Song, Shang, Song, & Wang, 2012). This fact favors the creation of WPU-CNC interactions (Rueda et al., 2013) as was also observed in FTIR and DSC results. Analyzing height images, in the case of 1 wt% nanocomposite, rod like CNC can be observed isolated from each other, whereas for 3 wt% an interrelated CNC mat can be appreciated, which can be related with the network structure. Nevertheless, in the case of 5 wt% some located agglomerates can be appreciated, being responsible of variations in the tendencies of the properties, as explained previously.

#### **4. Conclusions**

Waterborne polyurethane stable dispersion with high hard segment content was synthesized and employed for the preparation of nanocomposites with different CNC content, previously isolated from MCC, with an elevated L/D aspect ratio. DSC results revealed that low CNC content favored the crystallization of soft domains, while as CNC content was increased, in general, a progressive decrease in soft domains crystallization was observed due to the generation of WPU-CNC interactions, as observed by FTIR. Furthermore, by a theoretical approach, a theoretical percolation threshold about 3 wt% was estimated and was experimentally corroborated. Mechanical tests showed a considerable improvement in stress at yield and moduli values when the percolation threshold was reached, as well as DMA results which showed that the thermomechanical stability enhancement was more remarkable at CNC 3 wt%. However, above percolation threshold, at 5 wt% of CNC, a decrease in mechanical and thermomechanical properties was observed due to the formation of some located agglomerates which acted as failure points. The presence of those agglomerates in 5 wt% of CNC film as well as the homogeneous dispersibility of CNC in the matrix were corroborated by AFM. Furthermore, WCA and WA measurements revealed an increase of the hydrophilic character of the films along with CNC addition.

#### *Acknowledgements*

Financial support from the Basque Country Government in the frame of Grupos Consolidados (IT-776-13) and from the Spanish Ministry of Economy and Competitiveness (MINECO)(MAT2013-43076-R) is gratefully acknowledged. A. Santamaria-Echart whises to acknowledge the University of the Basque Country (UPV/EHU) for its PhD grant (PIF/UPV//12/201). Moreover, technical support provided by "Macrobehaviour-Mesostructure-Nanotechnology" and "Central Analysis of the UPV/EHU (Bizkaia)"SGIker units from the University of the Basque Country are also gratefully acknowledged.

## References

- Ashori, A., Babaee, M., Jonoobi, M., & Hamzeh, Y. (2014). Solvent-free acetylation of cellulose nanofibers for improving compatibility and dispersion. *Carbohydrate Polymers*, 102, 369–375.
- Auad, M. L., Mosiewicki, M. A., Richardson, T., Aranguren, M. I., & Marcovich, N. E. (2010). Nanocomposites made from cellulose nanocrystals and tailored segmented polyurethanes. *Journal of Applied Polymer Science*, 115, 1215–1225.
- Azizi Samir, M. A. S. A., Alloin, F., & Dufresne, A. (2005). Review of recent research into cellulosic whiskers: their properties and their application in nanocomposite field. *Biomacromolecules*, 6, 612–626.
- Beck, S., Bouchard, J., & Berry, R. (2012). Dispersibility in water of dried nanocrystalline cellulose. *Biomacromolecules*, 13, 1486–1494.
- Benhamou, K., Kaddami, H., Magnin, A., Dufresne, A., & Ahmad, A. (2015). Bio-based polyurethane reinforced with cellulose nanofibers: a comprehensive investigation on the effect of interface. *Carbohydrate Polymers*, 122, 202–211.
- Bullermann, J., Friebel, S., Salthammer, T., & Spohnholz, R. (2013). Novel polyurethane dispersions based on renewable raw materials-stability studies by variations of DMPA content and degree of neutralisation. *Progress in Organic Coatings*, 76(4), 609–615.
- Cao, X., Dong, H., & Li, C. M. (2007). New nanocomposite materials reinforced with flax cellulose nanocrystals in waterborne polyurethane. *Biomacromolecules*, 8, 899–904.
- Chattopadhyay, D. K., & Raju, K. V. S. N. (2007). Structural engineering of polyurethane coatings for high performance applications. *Progress in Polymer Science*, 32, 352–418.
- Dong, X. M., Revol, J. F., & Gray, D. G. (1998). Effect of microcrystallite preparation conditions on the formation of colloid crystals of cellulose. *Cellulose*, 5, 19–32.
- Eichhorn, S. J., Dufresne, A., Aranguren, M., Marcovich, N. E., Capadona, J. R., Rowan, S. J., . . . & Peijs, T. (2010). Review: current international research into cellulose nanofibres and nanocomposites. *Journal of Materials Science*, 45, 1–33.
- Framework convention on climate change (2015). In Adoption of the Paris agreement (Vol. L.9/Rev.1).
- Gaddam, S. K., & Palanisamy, A. (2016). Anionic waterborne polyurethane dispersions from maleated cotton seed oil polyol carrying ionisable groups. *Colloid and Polymer Science*, 294, 347–355.
- Gao, Z., Peng, J., Zhong, T., Sun, J., Wang, X., & Yue, C. (2012). Biocompatible elastomer of waterborne polyurethane based on castor oil and polyethylene glycol with cellulose nanocrystals. *Carbohydrate Polymers*, <http://dx.doi.org/10.1016/j.carbpol.2011.10.027>
- Gopiraman, M., Jatoi, A. W., Hiromichi, S., Yamaguchi, K., Jeon, H. Y., Chung, I.-M., & Kim, I. S. (2016). Silver coated anionic cellulose nanofiber composites for an efficient antimicrobial activity. *Carbohydrate Polymers*, <http://dx.doi.org/doi:10.1016/j.carbpol.2016.04.084>
- Habibi, Y., Lucia, L. a., & Rojas, O. J. (2010). Cellulose nanocrystals: chemistry, self-assembly, and applications. *Chemical Reviews*, 110(6), 3479–3500.
- Hribernik, S., Kleinscheek, K. S., Rihm, R., Ganster, J., Fink, H. P., & Smole, M. S. (2016). Tuning of cellulose fibres' structure and surface topography: influence of swelling and various drying procedures. *Carbohydrate Polymers*, <http://dx.doi.org/doi:10.1016/j.carbpol.2016.04.053>

- Hubbe, M. A., Gardner, D. J., & Shen, W. (2015). Contact angles and wettability of cellulosic surfaces: a review of proposed mechanisms and test strategies. *Bioresources*, 10(4), 8657–8749.
- Kunaver, M., Anzlovar, A., & Zagar, E. (2016). The fast and effective isolation of nanocellulose from selected cellulosic feedstocks. *Carbohydrate Polymers*, <http://dx.doi.org/doi:10.1016/j.carbpol.2016.04.076>
- Kushwaha, O. S., Avadhani, C. V., & Singh, R. (2014). Effect of UV rays on degradation and stability of high performance polymer membranes. *Advanced Materials Letters*, 5, 272–279.
- Kushwaha, O. S., Avadhani, C. V., & Singh, R. P. (2015). Preparation and characterization of self-photostabilizing UV-durable bionanocomposite membranes for outdoor applications. *Carbohydrate Polymers*, 123, 164–173.
- Leitsch, E. K., Heath, W. H., & Torkelson, J. M. (2016). Polyurethane/polyhydroxyurethane hybrid polymers and their applications as adhesive bonding agents. *International Journal of Adhesion and Adhesives*, 64, 1–8.
- Liu, H., Song, J., Shang, S., Song, Z., & Wang, D. (2012). Cellulose nanocrystal/silver nanoparticle composites as bifunctional nanofillers within waterborne polyurethane. *ACS Applied Materials and Interfaces*, 4, 2413–2419.
- Liu, H., Cui, S., Shang, S., Wang, D., & Song, J. (2013). Properties of rosin-based waterborne polyurethanes/cellulose nanocrystals composites. *Carbohydrate Polymers*, 96, 510–515.
- Ly, B., Thielemans, W., Dufresne, A., Chaussy, D., & Belgacem, M. N. (2008). Surface functionalization of cellulose fibres and their incorporation in renewable polymeric matrices. *Composites Science and Technology*, 68, 3193–3201.
- Mao, H., Qiang, S., Yang, F., Zhao, C., Wang, C., & Yin, Y. (2015). Synthesis of blocked and branched waterborne polyurethanes for pigment printing applications. *Journal of Applied Polymer Science*, 42780, 1–9.
- Mariano, M., El Kissi, N., & Dufresne, A. (2014). Cellulose nanocrystals and related nanocomposites: review of some properties and challenges. *Journal of Polymer Science Part B: Polymer Physics*, 52, 791–806.
- Mo, F., Zhou, F., Chen, S., Yang, H., Ge, Z., & Chen, S. (2015). Development of shape memory polyurethane based on polyethylene glycol and liquefied 4,4'-diphenylmethane diisocyanate using a bulk method for biomedical applications. *Polymer International*, 64(4), 477–485.
- Mondragon, G., Fernandes, S., Retegi, A., Pen˜a, C., Algar, I., Eceiza, A., & Arbelaitz, A. (2014). A common strategy to extracting cellulose nanoentities from different plants. *Industrial Crops and Products*, 55, 140–148.
- Nelson, A. M., & Long, T. E. (2014). Synthesis, properties, and applications of ion-containing polyurethane segmented copolymers. *Macromolecular Chemistry and Physics*, 215, 2161–2174.
- Pei, A., Malho, J., Ruokolainen, J., Zhou, Q., & Berglund, L. A. (2011). Strong nanocomposite reinforcement effects in polyurethane elastomer with low volume fraction of cellulose nanocrystals. *Macromolecules*, 44, 4422–4427.
- Rueda, L., Fernández d'Arlas, B., Zhou, Q., Berglund, L. A., Corcuera, M. A., Mondragon, I., & Eceiza, A. (2011). Isocyanate-rich cellulose nanocrystals and their selective insertion in elastomeric polyurethane. *Composites Science and Technology*, 71, 1953–1960.

- Rueda, L., Saralegui, A., Fernández, B., Zhou, Q., Berglund, L. A., Corcuera, M. A., . . . & Eceiza, A. (2013). Cellulose nanocrystals/polyurethane nanocomposites. Study from the viewpoint of microphase separated structure. *Carbohydrate Polymers*, 92(1), 751–757.
- Rueda, L., Fernandez d'Arlas, B., Corcuera, M. A., & Eceiza, A. (2014). Biostability of polyurethanes. Study from the viewpoint of microphase separated structure. *Polymer Degradation and Stability*, 108, 195–200.
- Santamaría-Echart, A., Arbelaitz, A., Saralegi, A., Fernández-d'Arlas, B., Eceiza, A., & Corcuera, M. A. (2015). Relationship between reagents molar ratio and dispersion stability and film properties of waterborne polyurethanes. *Colloids and Surfaces A: Physicochemical and Engineering Aspects*, 482, 554–561.
- Santamaria-Echart, A., Ugarte, L., Arbelaitz, A., Gabilondo, N., Corcuera, M. A., & Eceiza, A. (2016). Two different incorporation routes of cellulose nanocrystals in waterborne polyurethane nanocomposites. *European Polymer Journal*, 76, 99–109.
- Saralegi, A., Rueda, L., Martin, L., Arbelaitz, A., Eceiza, A., & Corcuera, M. A. (2013). From elastomeric to rigid polyurethane/cellulose nanocrystal bionanocomposites. *Composites Science and Technology*, 88, 39–47.
- Schön, P., Bagdi, K., Molnár, K., Markus, P., Pukánszky, B., & Vancso, G. J. (2011). Quantitative mapping of elastic moduli at the nanoscale in phase separated polyurethanes by AFM. *European Polymer Journal*, 47, 692–698.
- Si, H., Liu, H., Shang, S., Song, J., Liao, S., Wang, D., & Song, Z. (2016). Maleopimamic acid-modified two-component waterborne polyurethane for coating applications. *Journal of Applied Polymer Science*, 43292, 1–9.
- Tharcis, M., Badel, T., Jéol, S., Fleury, E., & Méchin, F. (2016). High elongation thermoplastic Polyester-urethanes based on widely available diacid intermediates. *Journal of Applied Polymer Science*, 43410, 1–15.
- Tuzzin, G., Godinho, M., Dettmer, A., & Zattera, A. J. (2016). Nanofibrillated cellulose from tobacco industry wastes. *Carbohydrate Polymers*, 148, 69–77.
- Wunderlich, B. (2005). Thermal analysis of polymeric materials Springer. Berlin, Heidelberg: Springer.
- Xiang, L. Y., Mohammed, M. A. P., & Baharuddin, A. S. (2016). Characterisation of microcrystalline cellulose from oil palm fibres for food applications. *Carbohydrate Polymers*, 148, 11–20.
- Yilgör, I., Yilgör, E., & Wilkes, G. L. (2015). Critical parameters in designing segmented polyurethanes and their effect on morphology and properties: a comprehensive review. *Polymer*, 58, A1–A36.
- Zhang, Y., Liu, Y., Wang, X., Sun, Z., Ma, J., Wu, T., . . . & Gao, J. (2014). Porous graphene oxide/carboxymethyl cellulose monoliths, with high metal ion adsorption. *Carbohydrate Polymers*, 101, 392–400.
- Zhou, Z., Peng, X., Zhong, L., Wu, L., Cao, X., & Sun, R. C. (2016). Electrospun cellulose acetate supported Ag@AgCl composites with facet-dependent photocatalytic properties on degradation of organic dyes under visible-light irradiation. *Carbohydrate Polymers*, 136, 322–328.

## Supplementary material A

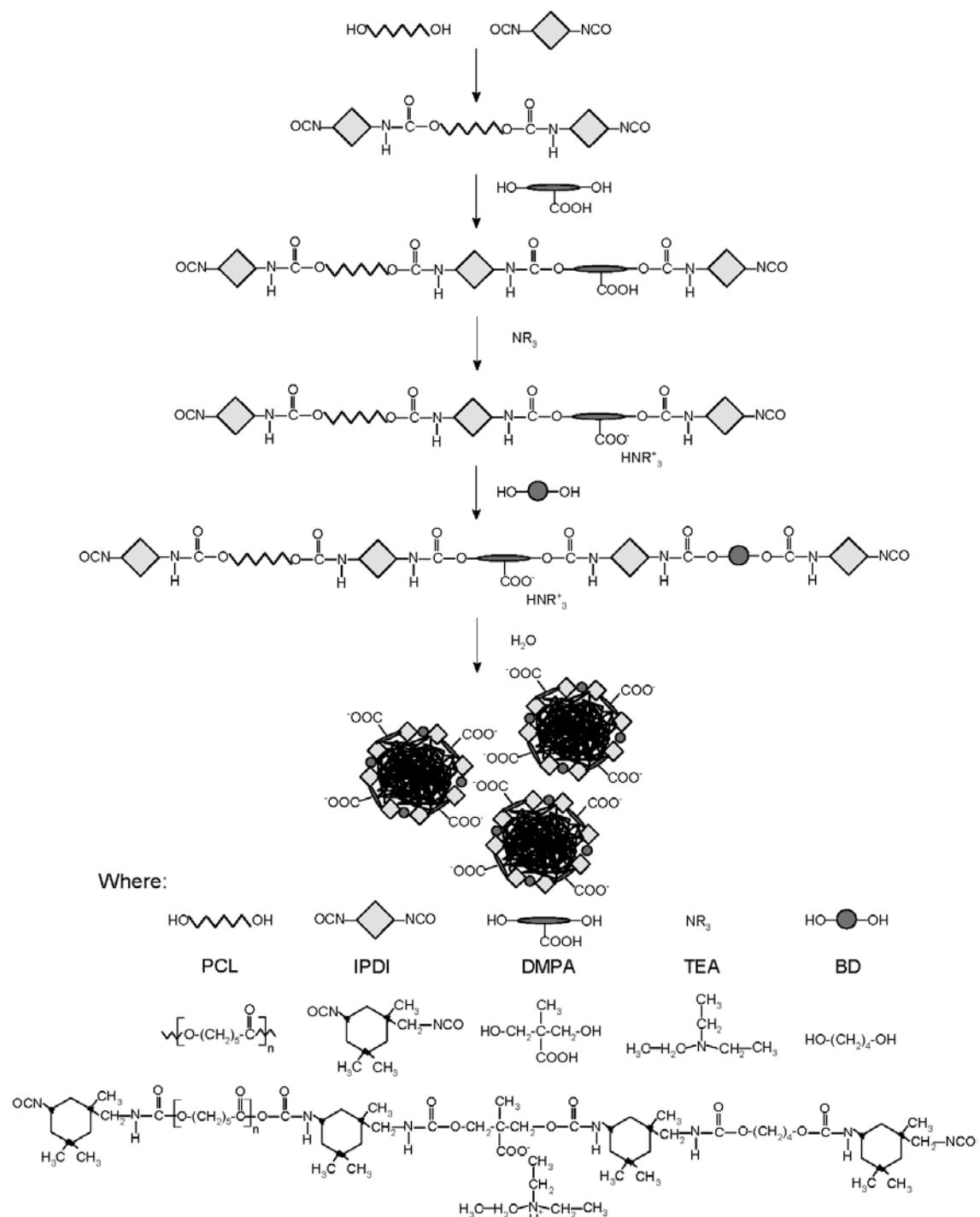


**Figure A1.** Scheme of the WBPU synthesis reaction process

The structure of the polyurethane was analyzed by  $^{13}\text{C}$  and  $^1\text{H}$  NMR and the spectra are shown in Figure A2 and A3, respectively. Regarding to  $^{13}\text{C}$  NMR results, the absence of NCO groups

peaks around 123-121 ppm indicate that the synthesis reaction proceed completely (Fu, Zheng, Yang, Chen, & Shen, 2014; Yong et al., 2015) and the peaks around 156 and 157 ppm implies the formation of urethane groups (Daemi, Barikani, & Barmar, 2013; Yong et al., 2015). The C=O carbonyl characteristic group of PCL soft segment is related with the peak at 173 ppm, whereas  $-\text{OCH}_2$  and  $-\text{CH}_2\text{COO}$  PCL groups carbons are attributed to the peaks at 63-64 and 34 ppm respectively (Rajkumar, Dhanalakshmi, Meenarathi, & Anbarasan, 2016). The rest of the PCL carbon groups are involved in the peaks between 30-40 ppm (Rajkumar et al., 2016). The peaks from 24 to 45 ppm are related with the methyl and skeleton of IPDI and DMPA carbons(Daemi et al., 2013; Yong et al., 2015) and that about 55 ppm is assigned to the IPDI carbon linked to urethane groups (Daemi et al., 2013). Moreover, the peak at 47 ppm indicates the presence of ethyl carbons of the triethylammonium form of TEA (Daemi et al., 2013).

The polyurethane structure was also analyzed by  $^1\text{H}$  NMR were the different peaks were assigned to the corresponding characteristic protons of the polyurethane backbone. The peaks at 6.95 and 7 ppm confirm the presence of urethane groups without the formation of allophanate NH groups, due to the absence of a peak at 7.52 ppm (Yong et al., 2015), which are generated by isocyanate side reactions during the synthesis. Considering SS, the peaks around 4, 2.3 and 1.55 and 1.3 ppm are related to PCL  $-\text{OCH}_2-\text{CH}_2\text{COO}$  and methylene groups' protons, respectively (Peng, Zhang, Chen, Li, & He, 2016). The peaks in the range between 0.8 and 1.6 ppm are assigned to methyl and ethyl protons in IPDI, DMPA and BD (Daemi et al., 2013; Yong et al., 2015) backbone whereas around 2.4-3.8 ppm IPDI protons near to urethane groups can be appreciated. Furthermore, TEA  $-\text{CH}_2$  group protons attached to tertiary amine nitrogen are observed about 3 ppm.

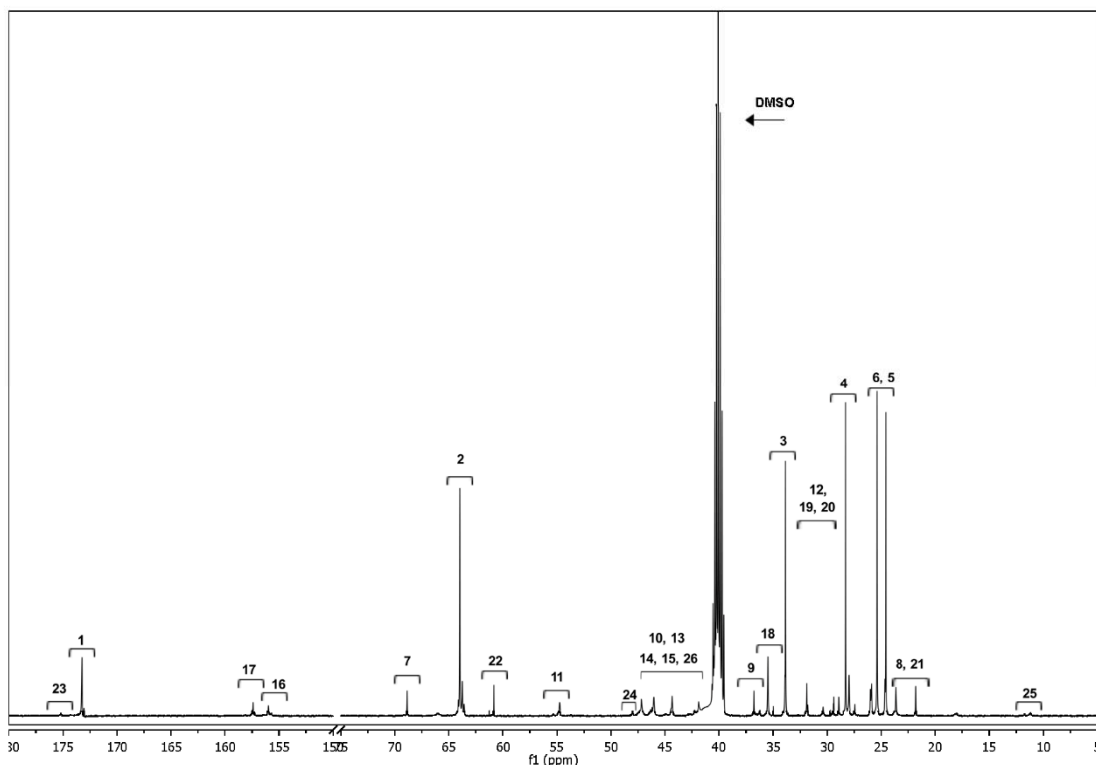
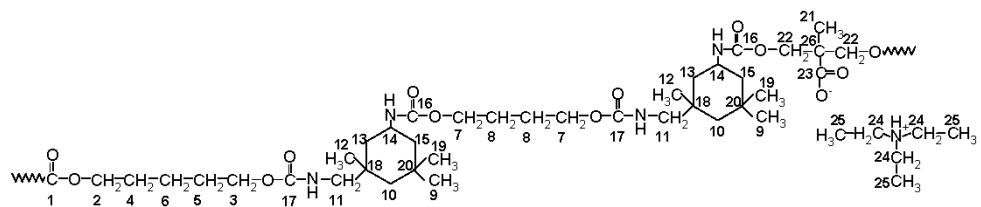


**Figure A2.**  $^{13}\text{C}$  NMR spectrum of WBPU. The measurement was carried out in a Bruker Avance 500 spectrometer, equipped with a BBO probe with gradient in Z axis. The spectrum was recorded using a decoupled sequence zgdc from Bruker library at 125.77 MHz. A time domain of 64k was used in a spectral width of 31000 Hz. An interpulse delay of 2s was employed for and acquisition time of 1.5 s averaging 32K scans.

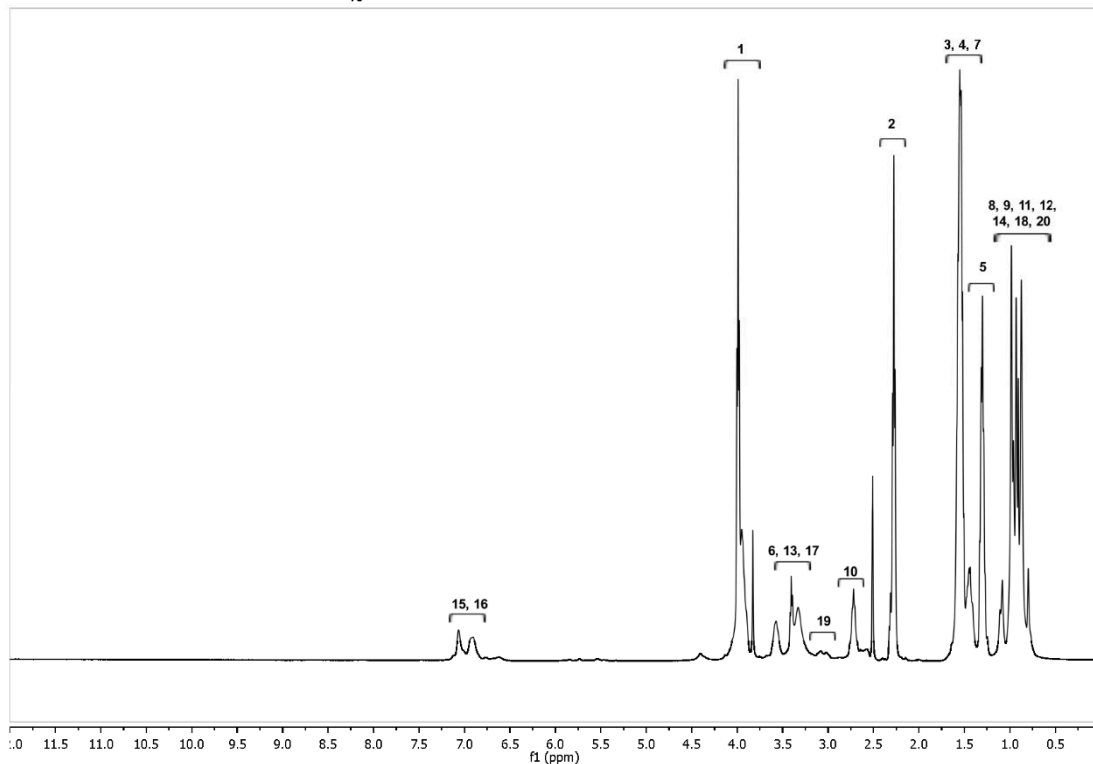
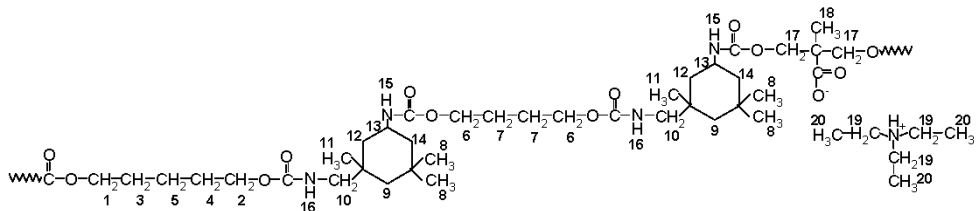


**Figure A3.**  $^1\text{H}$  NMR spectrum of WBPU. The measurement was carried out in a Bruker Avance 500 spectrometer, equipped with a BBO probe with gradient in Z axis. The spectrum was recorded using sequence zg Bruker library at 125.77 MHz. A time domain of 64K was used in a spectral width of 10000 Hz. An interpulse delay of 2 s was employed for and acquisition time of 3 s averaging 64K scans.

## References

- Daemi, H., Barikani, M., & Barmar, M. (2013). Compatible compositions base on aqueous polyurethane dispersions and sodium alginate. *Carbohydrate Polymers*, 92, 490–496.
- Fu, C., Zheng, Z., Yang, Z., Chen, Y., & Shen, L. (2014). A fully bio-based waterborne polyurethane dispersion from vegetal oils: From synthesis of precursors by thiol-ene to study of final material. *Progress in Organic Coatings*, 77, 53–60.
- Peng, X., Zhang, Y., Chen, Y., Li, S., & He, B. (2016). Synthesis and crystallization of well-defined biodegradable miktoarm star PEG-PCL-PLLA copolymer. *Materials Letters*, 171, 83–86.
- Rajkumar, B., Dhanalakshmi, T., Meenarathi, B., & Anbarasan, R. (2016). Synthesis and characterization of novel fluorescent amphiphilic diblock copolymer. *Polymer Bulletin*. doi:10.1007/s00289-016-1600-z.
- Yong, Q., Nian, F., Liao, B., Huang, L., Wang, L., & Pang, H. (2015). Synthesis and characterization of solvent-free waterborne polyurethane dispersion with both sulfonic and carboxylic hydrophilic chain-extending agents for matt coating applications. *RSC Advances*, 5, 107413–107420.